Wide Solitons in an Ion-Beam–Plasma System

S.-G. Lee, D. A. Diebold, N. Hershkowitz, and P. Moroz
Department of Nuclear Engineering and Engineering Physics, University of Wisconsin-Madison, Madison, Wisconsin 53706
(Received 28 December 1994)

Solitons are experimentally found in a double plasma device when an ion beam is present with beam velocity v_b in the range $1 \leq v_b/c_s \leq 2.2$, where c_s is the ion acoustic velocity. These one dimensional solitons have an unusually large width (parallel to the direction of propagation) $W \approx 14\lambda_D(\delta n/n)^{-1/2}$, where λ_D is the Debye length and $\delta n/n$ is the maximum normalized density fluctuation. The amplitude, width, and velocity characteristics of the solitons are found to be in good agreement with the soliton solution to the Korteweg–de Vries equation in an ion-beam–plasma system. [S0031-9007(96)00856-3]

PACS numbers: 52.40.Mj, 52.35.Mw, 52.35.Sb

The term "soliton" was coined by Zabusky and Kruskal [1] to describe pulselike solutions to the nonlinear Korteweg–de Vries (KdV) equation [2]. They showed that solitons have the following properties: the soliton velocity is proportional to the maximum normalized density fluctuation $\delta n/n$; solitons traveling in the same direction survive collisions with only a change of phase; $\delta n/n$ and the soliton width W parallel to the direction of propagation satisfy $(\delta n/n)W^2 = \text{const}$; and arbitrary initial compressive density perturbations evolve into one or more solitons.

Washimi and Taniuti [3] showed that weakly nonlinear ion acoustic waves, in stationary plasmas with one cold ion species, were described by the KdV equation. Since that Letter, there have been many experimental and theoretical studies of ion acoustic solitons in plasmas [3–14]. The KdV equation for a plasma with finite ion temperature was described by Tran [9]. Gell and Roth [10], building on the work of Tran, derived the KdV equation for a plasma containing an ion beam and background plasma. Here we report what we believe is the first experimental observation of soliton generation in an ion-beam–plasma system. The amplitude, width, and velocity characteristics of these solitons are in good agreement with the theory [10] and have the interesting feature that the product $(\delta n/n)W^2$, while still approximately constant, is much greater than for solitons in stationary plasmas.

Many soliton experiments have been carried out in double plasma (DP) devices [15]. Solitons are usually generated [4] in these devices by applying pulsed biases (approximately $T_e/2e$) between plasmas produced separately in two adjacent chambers. The applied pulsed biases create initial spatially localized density perturbations from which the solitons evolve. For the experiments presented here, the potentials of the source and target chamber plasmas were adjusted so that a steady beam of ions passed through the background plasma. This resulted in an instability, which in turn created the initial density perturbations from which the solitons evolved. Hence, the experiments presented here differ from previous soliton experiments in that there were beam ions as well as the stationary background ions.

The experiment described here was carried out in a triple plasma device [16] operated as a DP device. The plasma parameters for this experiment are the source chamber plasma density $n_e \approx 8 \times 10^8$ cm^{-3}, target chamber $n_e \approx (5–10) \times 10^7$ cm^{-3}, electron temperature $T_e \approx 1.5$ eV in both chambers, and the argon neutral pressure $\approx 3.5 \times 10^{-4}$ torr. Plasma is produced by energetic electrons emitted by hot filaments. In such filament discharge plasmas, the ion temperature T_i is typically an order of magnitude less than T_e [17]. The plasma production in this experiment differs from that of previous soliton experiments in that filaments are located in only one chamber (the source chamber) of the DP device rather than both chambers. The data were taken with a Hewlett-Packard 54512B oscilloscope. Plasma densities were measured with a 0.64 cm diameter, one-sided Langmuir probe biased at -60 V with respect to ground. Plasma potential measurements were made by emissive probes [18].

When the target chamber plasma potential ϕ_t in the DP device is adjusted to be $(0.5–2)T_e/e$ below the source chamber plasma potential ($\phi_s = +50$ V), a low frequency instability (≈ 2 kHz), much lower than the ion plasma frequency, is observed. Adjustment of ϕ_t is accomplished by varying the potential difference between the grid bias ($V_g = +10$ to $+15$ V) and filament bias ($V_f = 0$ V). The instability is not observed whenever $\phi_s - \phi_t < 0.5T_e/e$ or $> 2T_e/e$. We have measured this instability's dispersion relation and identified it as an ion-ion beam instability [19]. Representative data showing the temporal behavior of the target chamber ion density (determined from the ion saturation current) and the target chamber plasma potential ϕ_t (determined by an emissive probe) are given in Figs. 1(a) and 1(b). Note that $\phi_t(t)$ is approximately half-wave rectified. We will refer to the flat positive amplitude half of the cycle as the "plateau." During the plateau, ϕ_t is constant and is approximately 1.5 V less than the source chamber plasma potential ϕ_s, which

 0031-9007/96/77(7)/1290(4)$10.00

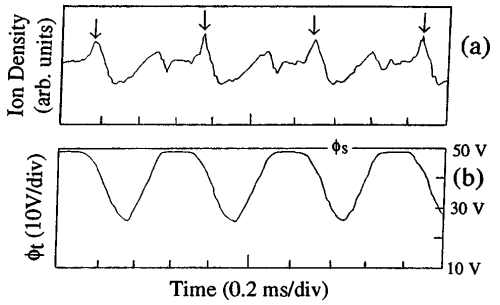

FIG. 1. (a) A typical example of the temporal behavior of the target chamber density (i.e., ion saturation current) showing the soliton (denoted by arrows) and the ion-ion beam instability associated with it (arb. units). (b) The corresponding temporal behavior of the target chamber plasma potential ϕ_t (10 V/div). Note that ϕ_t is saturated during the plateau of the ion-ion beam instability.

is fixed. Hence, during this time $\phi_s - \phi_t \approx 1.0T_e/e$ and in the target chamber there is an ion beam with energy $\approx$1.5 eV and normalized velocity $v_b/c_s \approx 1.4$. During the negative half of the instability cycle, ϕ_t varies with time in a sinusoidal fashion, decreasing by 20 V before coming back to the constant plateau potential. Solitons were observed at the trailing edges and, to a lesser extent, at the leading edges of plateaus [as seen in Fig. 1(a)].

Figure 2 shows soliton density on [as compared to Fig. 1(a)] an enlarged scale. Ion density vs time is shown in Fig. 2 at various axial positions. The grid is located at $z = 0$. For clarity, the densities shown at the various z are vertically displaced from one another in the figure and a vertical line is drawn through the peak in density at $z = 9$ cm. As can be seen from Fig. 1, there was significant variation in the amplitudes and widths of the solitons observed at a given axial location. The data shown in Fig. 2 are the average of the data taken from 100 triggerings of the oscilloscope. Two soliton characteristics can be qualitatively seen in the data of Fig. 2: As the soliton amplitude increases (with increasing z), the velocity of the soliton increases and the width of the soliton decreases.

To quantitatively compare the observed soliton characteristics with theory, consider the KdV equation [2] for an ion-beam–plasma system [9,10]:

$$\frac{\partial n_e^{(1)}}{\partial \tau} + P n_e^{(1)} \frac{\partial n_e^{(1)}}{\partial \xi} + \frac{1}{2} Q \frac{\partial^3 n_e^{(1)}}{\partial \xi^3} = 0, \qquad (1)$$

where $n_e^{(1)}$ is the first order perturbation of the electron density, τ is the time normalized by the ion plasma frequency ($\tau = \omega_{pi} t$), ξ is the spatial coordinate measured in units of the electron Debye length ($\xi = z/\lambda_D$), and P and Q depend on the plasma parameters and the phase velocity of linear waves in the system [9,10]. The solution of Eq. (1) yields a solitary wave pulse

$$n_e^{(1)} = \delta n \, \mathrm{sech}^2[(z - v_{\mathrm{soliton}} t)/W], \qquad (2)$$

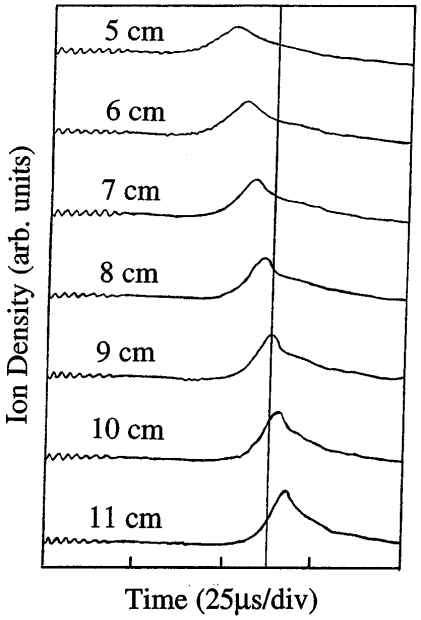

FIG. 2. Ion density (arb. units) associated with soliton vs time (25 μs/div) at various axial position z (cm). With increasing z, the width of the soliton decreases while its amplitude increases. For clarity, the densities shown at the various z are vertically displaced from one another in the figure and a vertical line is drawn through the peak in density at $z = 9$ cm. The data shown in this figure are the average of the data taken from 100 triggerings of the oscilloscope.

where W is the width of the soliton and δn is the amplitude of the soliton. The product of the width and amplitude satisfy

$$\frac{\delta n}{n} \left(\frac{W}{\lambda_D} \right)^2 = 6 \frac{P}{Q} \qquad (3)$$

and

$$v_{\mathrm{soliton}} = u \left[1 + \frac{1}{3} \frac{\delta n}{n} \frac{1 + 6\theta_i}{(1 + 3\theta_i)^{3/2}} \right], \qquad (4)$$

where θ_i is the ratio of ion to electron temperature and u is the phase velocity of linear waves. Equations (3) and (4) are the quantitative soliton characteristics to which the data will be compared.

To compare the data with Eqs. (3) and (4), the phase velocity u must be known as P, Q, and v_{soliton} depend on u. Figure 3 shows the calculated dispersion relation of the ion-beam–plasma system [10] corresponding to this experiment. Solid lines are the real parts and dotted lines are the imaginary parts of the solutions. For $v_b/C_s \geq 2.2$, the branches can be identified as the "fast beam mode," "slow beam mode," and "plasma" branches, and for $v_b/C_s \leq 2.2$, the branches can be identified as the fast beam mode and the "unstable mode." The observed solitons can be identified with the unstable mode branch of the dispersion relation. Only the real part of this branch was used in the calculation of P and Q; the imaginary part was assumed to be insignificant.

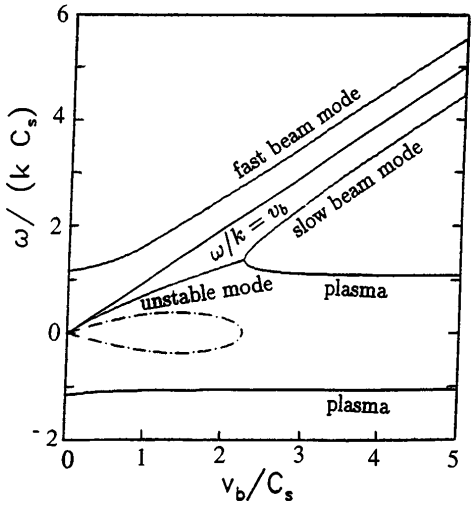

FIG. 3. Analytically calculated dispersion relation in an ion-beam–plasma system. All solid lines (except $\omega/k = v_b$) are real parts and dotted lines are imaginary parts of the solutions of the ion-ion dispersion relation.

Results of the calculation of $6(Q/P)$ are shown in Fig. 4. Following prescriptions given in Refs. [9,10], Fig. 4 shows $6(Q/P)$ vs v_b/C_s when $\mu = 1$ (where μ is the plasma ion to beam ion mass ratio), the beam ions are cold (i.e., their temperature is small enough that it can be neglected), $\theta_i \approx 0.1$ and $\alpha \approx 0.25$, where α is the ratio of unperturbed ion beam density to electron density. Note that these are the parameters of the experiment and are typical of the conditions for the observations being discussed. As can be seen in Fig. 4, P and Q values have three distinctive regions, $v_b/C_s \approx 0$, $0.7 \leq v_b/C_s \leq 1.7$, and $v_b/C_s > 2$. When $v_b/C_s \approx 0$ or >2, $6(Q/P) \approx 6$ and Eq. (1) admits the usual ion acoustic soliton solution.

The parameter v_b/C_s varies throughout the instability cycle. During the plateau, ϕ_t saturates at a value approximately T_e/e below the source potential. The corresponding normalized velocity is $v_b/C_s \approx 1.4$, which is both in the unstable regime (shown as the dotted lines in Fig. 3) and in the regime corresponding to the maximum value of $6(Q/P) \approx 200$ (see Fig. 4). At the end of the plateau, a drop in ϕ_t of approximately 20 V begins. We note that the plateau lifetime is approximately the transit time across the target chamber of ions with $v_b/C_s \approx 1.4$, i.e., the drop in ϕ_t begins at about the time that the first ions to enter the target chamber during the plateau cycle reach the end of the target chamber. Further, the drop in ϕ_t lasts for approximately the same amount of time, i.e., the minimum in ϕ_t occurs at approximately the time that the last ions to enter the target chamber during the plateau cycle reach the end of the target chamber. At the ϕ_t minimum, $v_b/C_s \approx 5$, which is in the stable regime. The potential recovers and once again enters the plateau phase of the instability cycle.

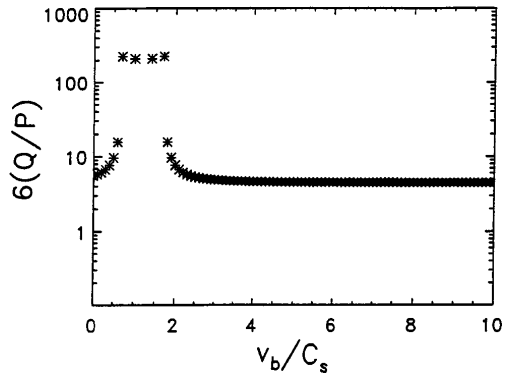

FIG. 4. Calculated $6(Q/P)$ vs v_b/C_s.

The value of v_b/C_s is in the range corresponding to the maximum value of Q/P during the plateau and during the leading and trailing edges of the plateau, but not during most of the negative half of the instability cycle. The solitons shown in Fig. 1 begin at approximately the times at which the potential first starts to drop from its plateau value. The peaks in the solitons occur approximately at the time when the value of v_b/C_s leaves the regime of maximum Q/P. Specifically, $6(Q/P) \approx 200$ until the potential drops to approximately 3 V below the source potential ($\phi_s = 50$ V), i.e., until v_b/C_s becomes greater than approximately 2. As the trailing edge occurs when $\phi_s - \phi_t > 3$ V [and, hence, $6(Q,P) < 200$], we measure the width of the soliton between the peak and the leading (left) edge of the soliton rather than between the peak and the trailing edge or between the leading edge and the trailing edge.

Normalized soliton amplitude and width data are shown in Fig. 5. As was noted above, there was significant variation in the amplitudes and widths of the solitons observed at a given axial location (e.g., see Fig. 1). To arrive at the data shown in Fig. 5, the amplitudes and widths of 100 solitons at each axial location were averaged.

In Fig. 5, the ○'s show the product of normalized soliton amplitude and width squared $[(\delta n/n)W^2/\lambda_D^2]$,

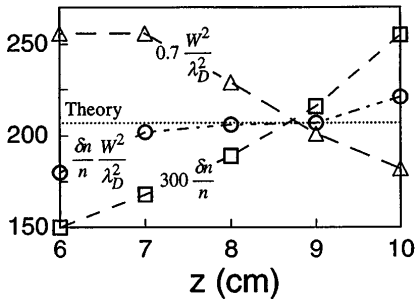

FIG. 5. The ○'s show the product of normalized soliton amplitude and width squared $[(\delta n/n)W^2/\lambda_D^2]$ vs axial position Z. The dotted line shows the theoretical soliton solution in the ion-beam–plasma system for which the soliton is observed. The □'s show $300\delta n/n$ vs Z and the △'s show $0.7W^2/\lambda_D^2$ vs Z. The $(\delta n/n)W^2/\lambda_D^2$ data are in good quantitative agreement with the theory and vary less than the $\delta n/n$ and W^2/λ_D^2 data.

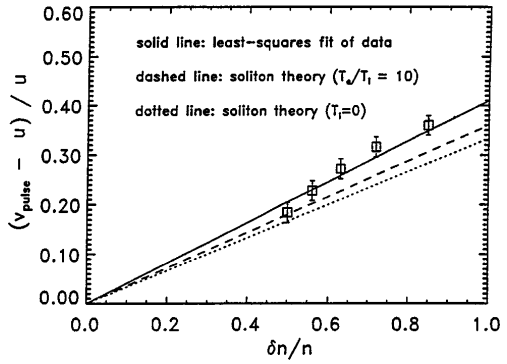

FIG. 6. The soliton velocity as a function of its amplitude. The solid line is a least-squares fit of measured data. The dotted ($T_i = 0$) and dashed ($T_e/T_i = 10$) lines are calculated from the soliton theory.

the □'s show $300\delta n/n$, and the △'s show $0.7W^2/\lambda_D^2$. The density n was taken to be directly proportional to the current drawn by the negatively biased Langmuir probe at a time just prior to the onset of the soliton, while δn was taken to be the difference between this n and the density when the soliton peaked. The reader may wish to note that n monotonically decreased from approximately 6.5×10^8 cm^{-3} at $z = 6$ to 4.5×10^8 cm^{-3} at $z = 10$. The soliton width W was taken to be the half width (between the peak and left side of the soliton) at 0.42 of peak, i.e., where sech^2 is half its maximum value. The dotted line shows the theoretical soliton solution in the ion-beam–plasma systems for which the soliton is observed. As can be seen from Fig. 5, the $(\delta n/n)W^2/\lambda_D^2$ data are in good quantitative agreement with the theoretical soliton solution [Eq. (3) with $6(Q/P) \approx 200$] in the ion-beam–plasma system. As can also be seen from Fig. 5, the $(\delta n/n)W^2/\lambda_D^2$ data vary less than the $\delta n/n$ and W^2/λ_D^2 data.

Note that this soliton has an unusually large width as compared to the width of an ion acoustic soliton in a stationary plasma without an ion beam. From Eq. (3) with $6(Q/P) \approx 200$, the width of the soliton shown here is $\approx 14\lambda_D(\delta n/n)^{-1/2}$ whereas that for an ion acoustic soliton in a stationary plasma without an ion beam [$6(Q/P) \approx 6$] is $\approx 2.5\lambda_D(\delta n/n)^{-1/2}$.

The data quantitatively agree with Eq. (4) as well. Figure 6 shows $(v_{\text{soliton}} - u)/u$ vs $\delta n/n$. The data were fit by assuming the u of the unstable mode. The relations [see Eq. (4)] between a soliton's velocity and its $\delta n/n$ as derived from the KdV equation are shown by the dotted ($T_i = 0$) and dashed ($T_e/T_i = 10$) lines in Fig. 6. The solid line in Fig. 6 is a least-squares fit to the measured data. As can be seen in Fig. 6, the v_{soliton} and $\delta n/n$ data are in good quantitative agreement with Eq. (4).

This work was supported by NSF Grant No. ATM-9017451.

[1] N. J. Zabusky and M. D. Kruskal, Phys. Rev. Lett. **15**, 240 (1965).
[2] D. J. Korteweg and G. de Vries, Philos. Mag. **39**, 422 (1895).
[3] H. Washimi and T. Taniuti, Phys. Rev. Lett. **17**, 996 (1966).
[4] H. Ikezi, R. J. Taylor, and D. R. Baker, Phys. Rev. Lett. **25**, 11 (1970).
[5] N. Hershkowitz, T. Romesser, and D. Montgomery, Phys. Rev. Lett. **29**, 1586 (1972).
[6] H. Ikezi, Phys. Fluids **16**, 1668 (1973).
[7] N. Hershkowitz and T. Romesser, Phys. Rev. Lett. **32**, 581 (1974).
[8] K. Lonngren, Plasma Phys. **25**, 943 (1983).
[9] M. Q. Tran, Plasma Phys. **16**, 1167 (1974).
[10] Y. Gell and I. Roth, Plasma Phys. **19**, 915 (1977).
[11] G. P. Zank and J. F. McKenzie, J. Plasma Phys. **39**, 183 (1988).
[12] L. Hubin and K. Wang, J. Plasma Phys. **44**, 151 (1990).
[13] C. Y. Zhang and H. H. Kuehl, Phys. Fluids **4**, 2517 (1992).
[14] C. Y. Zhang and H. H. Kuehl, Phys. Fluids **4**, 3185 (1992).
[15] R. J. Taylor, K. R. McKenzie, and H. Ikezi, Rev. Sci. Instrum. **43**, 1675 (1972).
[16] N. Hershkowitz, G. L. Payne, C. Chan, and J. R. DeKock, Plasma Phys. **23**, 903 (1981).
[17] R. J. Taylor and F. V. Coroniti, Phys. Rev. Lett. **29**, 37 (1972).
[18] R. F. Kemp and J. M. Sellen, Rev. Sci. Instrum. **37**, 455 (1966).
[19] S.-G. Lee, Ph.D. Thesis, University of Wisconsin-Madison, 1994.